PCCP

Accepted Manuscript

ROYAL SOCIETY OF CHEMISTRY

www.rsc.org/pccp

Insight into the Electronic Effect of Phosphine Ligand on Rh Catalyzed CO_2 Hydrogenation by Investigating the Reaction Mechanism

Shao-Fei Ni, Li Dang*

Department of Chemistry in Southern University of Science and Technology, Shenzhen, 518055, P. R. China

E-mail: dang.l@sustc.edu.cn

Keywords: *Density functional theory. CO2 Hydrogenation. Outer Coordination Sphere Effect. Thermodynamic hydricity.*

Abstraction

Catalytic efficiency of CO_2 hydrogenation is a big challenge in catalysed CO_2 recycling and H_2 conservation. Detailed mechanism of $[Rh(PCH_2X^RCH_2P)_2]^+$ (X^R = CH_2, N-CH_3, CF_2) catalyzed CO_2 hydrogenation is studied to obtain the insight into the electronic effect of the substituents at diphosphine ligand on the catalytic efficiency. The most favorable reaction mechanism is found to be composed by three steps: 1) Oxidative addition of dihydrogen onto the Rh center of the catalyst; 2) the first hydride abstraction by base from the Rh dihydride complexes; 3) the second hydride transfer from the Rh hydride complexes to CO_2. It was found that the transition state for the first hydride abstraction from Rh dihydride complex is the TOF-determining transition state (TDTS) in the most favorable mechanism. The energetic span (δE) of the cycle is suggested related to the thermodynamic

hydricity of the Rh dihydride complex. Model catalyst $[Rh(PCH_2CF_2CH_2P)_2]^+$ with strong σ electron withdrawing group on the diphosphine ligand provids higher hydricity in Rh dihydride complex and lower activation energy when compared with the other two catalysts. Our study shows that it is the σ electron withdrawing ability rather than the electron donating ability that enhanced the catalytic efficiency in catalyzed CO_2 hydrogenation. This finding will benefit the ligand design in transition metal catalyst and lead to more efficient methods for CO_2 transformation.

1. Introduction

More and more CO_2 is producing with the development of human industry, which greatly influences the environment and climate by destroying the carbon cycle.[1,2] People also noticed that CO_2 can be used as one of the renewable energy sources due to the vast amount of carbon resource and low cost.[3,4] Therefore, CO_2 fixation and conversion has attracted substantially increased scientific and industrial attention. Till now, a lot of CO_2 conversions leading to useful chemicals or fuels have been achieved.[5,6,7] The shortcoming in traditional CO_2 transformation methods is high cost, low yield and low efficiency, which inspires people to utilize and develop catalysts to solve these problems. Biomimetic enzyme as catalyst for the CO_2 conversion was used for a long time, but found with low yield[8] until an efficient whole-cell catalyst was reported by V. Müller in 2013.[9] With the coming of hydrogen economy tide, the hydrogenation of CO_2 to produce formic acid or formate is considered to be a "win-win" method: on the one hand, CO_2 is consumed; on the other hand, hydrogen is stored in transportable liquid state. In addition, formic acid and its salts are widely used in a variety of chemical, pharmaceutical, and industry areas. In fact,

the actual discovery of the possibility to synthesize formates from CO_2 and H_2 in the presence of bases and Pd as a catalyst dates back to 1914 by Carter et al.[10] In1935, the reaction was also realized by Adkins et al. with heterogeneous Raney nickel as the catalyst.[11] In mid-1970s, Hashimoto et al. firstly used the famous Wilkinson catalyst $RhCl(PPh_3)_3$ and the Ru analogue $RuCl(PPh_3)_3$ to catalyze the homogeneous hydrogenation of CO_2.[12] Precious metals Ru-[13,14,15,16], Rh-[17,18,19,20,21],and Ir-based[,22,23,24]catalysts are always been listed among the most active catalysts for CO_2 hydrogenation. A great breakthrough of unprecedented TON (3,500,000) and TOF(150,000 h^{-1}) was achieved by using the Ir(III) as the metal center of the catalyst by Nozaki et al. in 2009.[23] An unprecedented reaction rate of 1,892,000 h^{-1} at 132 ℃ was also realized Ru-PNP catalyst in combination with the strong DBU base by Filonenko et al.[30] Nonprecious metal catalysts are not often investigated due to the relatively low activity until 2011, Milstein et al. reported that the trans-[(tBu-PNP)Fe$(H)_2$(CO)] catalyst showed similar activity to most of the noble metal catalysts.[25] A lot of theoretical studies were also reported to investigate the catalyzed reaction mechanism.[26_35]

In recent years, more and more attention has been shifted to use different ligands or to change the second/outer coordination spheres of the ligands so that the catalytic efficiency will be enhanced.[36_41] In 2011, Hazari et al. demonstrated that CO_2 insertion process was facilitated by including a hydrogen bond donor in the second coordination sphere.[36] Another report in 2012 by Himeda and Fujita et al. showed that CO_2 hydrogenation efficiency was relied on the electronic effect of second coordination sphere.[38] Later, they proposed that a pendant base in the second sphere was good to the deprotonation of the

bidentate hydride, thus increasing the reaction efficiency.[39] In 2014, Linehan and Shaw et al. studied $[Rh(PCH_2X^RCH_2P)_2]^+$ (X^R = CH_2, N-CH_3, Amino Acids) catalyzed CO_2 hydrogenation and observed different catalytic activity with different substitutes at the outer coordination sphere of the bidentate phosphine ligand (Scheme 1).[42] Among these ligands, N-CH_3 substituted ligand was found giving the greatest enhancement to the catalytic efficiency of the reaction. The electron donating ability of N-CH_3 group is proposed as the key factor to increase the catalytic activity. In addition, Kubiak et al. reported another diphosphine complexes $[Rh(P_2N_2)_2]^+$ and the catalytic activity for CO_2 hydrogenation was examined at 2 atm and 21°. Similar mechanism is proposed and the amino group is also considered as an electron donating group.[37] However, people have little theoretical investigations on how the substituents at phosphine ligand affect the catalytic activity of metal phosphine complexes.[34,36–40] Here, we are interested in the detailed reaction mechanism and the electronic effect of the substitutes at the outer coordination sphere of the bidentate phosphine ligand. Therefore, density functional theory calculations were carried out to investigate the detailed reaction mechanism of $[Rh(PCH_2X^RCH_2P)_2]^+$ catalyzed CO_2 hydrogenation. Besides the catalysts $[Rh(PCH_2CH_2CH_2P)_2]^+$ (**A1)** and $[Rh(PCH_2N^{Me}CH_2P)_2]^+$ (**B1)** used in the experiment, catalyst model $[Rh(PCH_2CF_2CH_2P)_2]^+$ (**C1)** was also investigated in order to compare with **A1** and **B1**.

Scheme 1

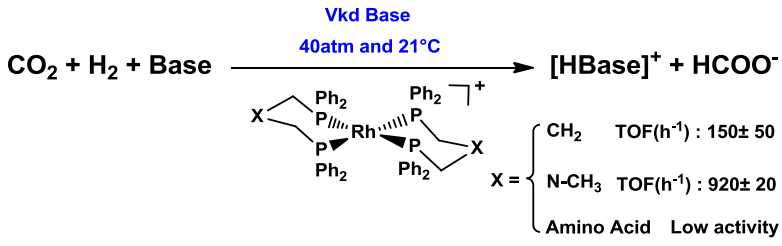

2. Computational Details

In current paper, calculations were performed at the ω-B97XD[43] functional using the Gaussian 09 program[44]. The effective core potentials (ECPs) of Hay and Wadt with a double-ζ valence basis set (LanL2DZ) were used for Rh and P[45,46,47,48], polarization functions were also added for Rh (f = 1.350) and P (f = 0.387) [49,50], whereas the all-electron 6-31++G** basis set was used in describing all other atoms.[51,52,53] To reduce the computational cost, model diphosphine ligands are used in which the phenyl groups attached to P atoms are replaced by the methyl groups. The similar simplification is often applied in phosphine ligands previously.[54,55,56,57,58] Geometric structures of all species in this paper were optimized as gas phase. The harmonic vibrational frequencies and the number of imaginary frequencies confirmed the nature of all intermediates (no imaginary frequency) and transition state structures (only one imaginary frequency). The latter were also confirmed to connect appropriate intermediates, reactants, or products by intrinsic reaction coordinate (IRC) calculations.[59,60] The gas-phase Gibbs free energies, *G*, were calculated at T = 298.15 K and 1 atm pressure within the harmonic potential approximation at optimized structures. Based on the gas phase optimized geometries, the solvation effect of tetrahydrofuran were simulated by the IEFPCM solvent model with the united atom topological model (UAKS) applied on radii.[61] The UAKS has been shown to work well

with the prediction of the thermodynamics properties for CO_2 hydrogenation by Yang.[27] The solution phase Gibbs free energy are calculated by adding solvation energies on the gas phase relative Gibbs free energies. The same methodology has been widely used in many recent theoretical works. [62 70] The thermodynamic hydricities of rhodium dihydride complexes are calculated based on the Fu and Liu's strategy.[71] The IEFPCM (UAKS radii) model with acetonitrile as solvent is used during the calculation of thermodynamic hydricities. The 3D molecular structures of all the species shown in the Supporting Information were drawn by using the CYLview program.[72] We examined the reaction of CO_2 with hydrogen in **Eq. 1**. In the experiment, the reaction of CO_2 with dihydrogen to give formate is endergonic ($\Delta G^o \approx 7.9$ kcal/mol) in gas phase and exergonic ($\Delta G^o \approx -1.0$ kcal/mol) in aqueous phase.[73] In our calculation, the calculated ΔG^o_{Rxn} for equation 1 is -13.0 kcal/mol in solution phase, which is consistent with the experiment tendency, showing the computational methods in this work are reliable.

$$CO_2 + H_2 + Base \rightarrow [HBase]^+ + HCOO^- \qquad \textbf{Eq. 1}$$

3. Results and Discussion

Preliminary investigation is carried out to test our model and calculation methods used here. The optimized geometry parameters of $[Rh(Me_2PCH_2N^{Me}CH_2PMe_2)_2]^+$ **(B1)** and $[Rh(Ph_2PCH_2N^{Me}CH_2PPh_2)_2]^+$ **(B1′)** were compared with that from the x-ray crystal structure in Table S1 (Supporting Information). It is found that the theoretical optimized geometry parameters of **B1** are closer to the X-ray crystal structure[42] than those of **B1′**. The steric effect in gas phase $[Rh(Ph_2PCH_2N^{Me}CH_2PPh_2)_2]^+$ **(B1′)** is larger than that in solution

phase and the replacement of Ph groups by Me reduces the steric effect in gas phase, making the simulation more reasonable. These results indicate that the model catalysts and the calculation methods used here are reliable.

Proposed reaction pathways for Rh(diphosphine)$_2$ catalyzed CO_2 hydrogenation are shown in Scheme 2, where reaction begins with the addition of H_2 to 16e Rh(I) center to form the 18e dihydride Rh(III) complex. Once the dihydride complex formed, the reaction falls into two general categories, the inner sphere pathway (Pathes 1 and 2**)**, and the outer sphere pathway (Path 3). For the inner sphere mechanism, by the nucleophilic attack of Verkade's base or the electrophilic attack of CO_2 to Rh(III) dihydride, the reaction proceeds either via Path 1 or via Path 2 to complete the catalytic cycle. It is worth emphasizing that the inner sphere Path 1 and Path 2 are universal for both X = CH_2, N-CH_3, and CF_2. Path 3 (X = N-CH_3) is the outer sphere route in which one hydride in the Rh(III) dihydride complex transfers to the outer sphere N atom, followed by the attack of Verkade's base or CO_2 to hydride on metal center or proton on amine group to reproduce the catalyst. Detailed reaction energy profiles along with these general pathways for **A1**, **B1**, and **C1** catalyzed CO_2 hydrogenation will be shown in the following discussion. Unless otherwise noted, the calculated solvation corrected relative Gibbs free energies ΔG_{sol} (kcal/mol) are presented in the figures and discussed in this paper. The relative Gibbs free energies ΔG_{gas} (kcal/mol), relative electronic energies ΔE_{gas} in gas phase (kcal/mol) and relative electronic energies ΔE_{sol} in solution phase (kcal/mol) are listed in SI.

Scheme 2. Outline of Predicted Reaction Mechanism for CO_2 Hydrogenation Catalyzed by $[Rh(PCH_2X^RCH_2P)_2]^+$ (X^R = CH_2, N-CH_3, and CF_2)

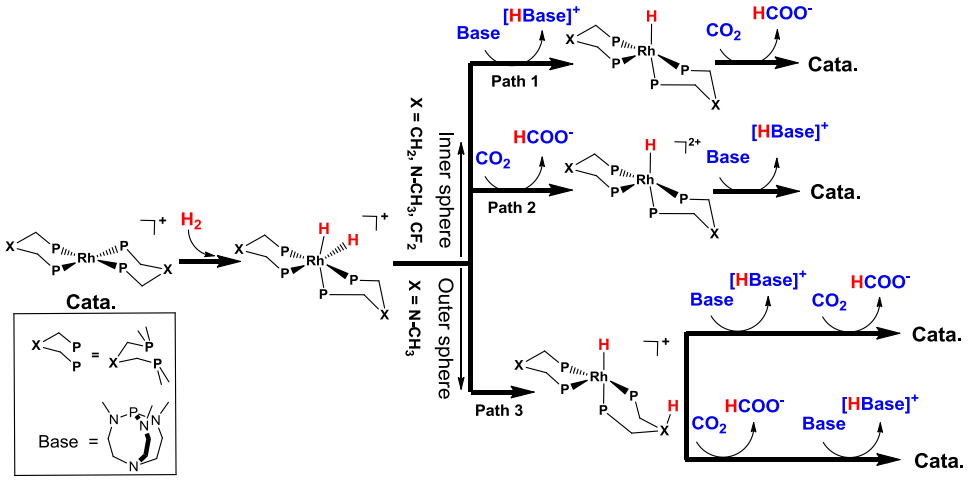

3.1. $[Rh(PCH_2CH_2CH_2P)_2]^+$ (A1) catalyzed CO_2 hydrogenation

$[Rh(PCH_2CH_2CH_2P)_2]^+$ (A1) catalyzed CO_2 hydrogenation begins with the H_2 oxidative addition. The energy profiles for two inner sphere based reaction pathways are shown in Figures 1 and 2**.** In Figure 1, the oxidative addition of H_2 on **A1** gives a 18e six-coordinated Rh(III) dihydride intermediate **A2** through transition state $\mathbf{TS_{A1\text{-}2}}$. The Gibbs free energy barrier for this H_2 oxidative addition process is 8.6 kcal/mol. Here, the pre-coordinate of H2 to A1 leads to the unstable sigma-complex $\mathbf{A1\text{-}H_2}$, which is higher in the solvent corrected Gibbs free energy than that of $\mathbf{TS_{A1\text{-}2}}$. This may be due to the overestimation of entropy effect because the calculated gas phase electronic energy of $\mathbf{A1\text{-}H_2}$ is only 0.3 kcal/mol lower than that of $\mathbf{TS_{A1\text{-}2}}$. The slightly unstable dihydride intermediate **A2** can be deprotonated by the nucleophilic attack of an external Verkade's base to form an unstable Rh(I) monohydride intermediate **A5**. The reaction barrier for this first hydride abstraction process is 29.1 kcal/mol, which is about 20.0 kcal/mol higher than that for H_2 oxidative addition. From the unstable five coordinated Rh(I) monohydride **A5**, CO_2 attackts the remaining hydride by insertion into the electron rich Rh-H σ bond through two definitely

different routes as shown in Scheme 3. One is a "direct" hydride abstraction route based on the weak interaction between the hydride and carbon atom of CO_2 (Scheme 3A). The other is the "normal" CO_2 insertion mode (Scheme 3B) in which CO_2 coordinates with Rh center first and then nucleophilic attack of metal hydride σ bond to CO_2 occurs. The last part of Figure 1 shows that the "direct" intermolecular hydride transfer happens via a transition state $\mathbf{TS_{A6\text{-}7}}$ with a barrier of 21.2 kcal/mol to give a metal formate intermediate **A7**. In "normal" CO_2 insertion mode, CO_2 occupies the empty coordination site of Rh center by overcoming a barrier of 19.8 kcal/mol and the nucleophilic attack of metal hydride bond to electron deficient CO_2 has a barrier of 19.2 kcal/mol. **A7** can also be formed after "normal" CO_2 insertion. The CO_2 insertion step via the "direct" hydride abstraction mode and the "normal" CO_2 insertion mechanism are comparable. Here, the metal formate intermediate **A7** has two different forms, the H-bound (Rh-(η^1-HCOO)) and O-bound (Rh-(η^1-OCOH)) metal formate, which have been reported and the rearrangement between these two structures is common.[27,32] Once the η^1-formate intermediate **A7** forms, the succeeding barrierless release of formate with protonated base occurs rapidly and leads to the catalyst regeneration.

From Figure 1, **A1** is the resting state of the catalytic cycle. According the energetic span concept introduced by Kozuch and Shaik [74,75,76,77], **A1** is the TOF-determining intermediate (TDI) and $\mathbf{TS_{A3\text{-}4}}$ for the abstraction of the first hydride from Rh dihydride complex is the TOF-determining transition state (TDTS) in Figure 1. The energetic span (δE) between the TDI and TDTS is calculated to be 29.1 kcal/mol.

However, another possibility to finish the catalytic cycle is that σ-bond metathesis[19,20] occurs between Rh-OCHO in **A7** and H_2 followed by CO_2 releasing to give **A5**. We studied this pathway and found there is a barrier of 18.8 kcal/mol (Figure S1) for this σ-bond metathesis to regenerate **A5**, which is comparable to the one in Figure 1 to regenerate **A1**. But in this new pathway, the formation of **A5** is very important, which cost 29.1 kcal/mol energy. Although **A5** can catalyze the CO_2 hydrogenation, the formation of **A5** is very difficult and **A5** is unstable. That's why **A5** was not observed and $PCH_2CH_2CH_2P$ ligand gives low TOF in the experiment.

Another pathway in which the first hydride of Rh dihydride complex is abstracted by CO_2 and the second one by base to regenerate the catalyst was also studied. The calculated results of this route are shown in Figure 2. From the dihydride Rh(III) complex **A2**, a hydride transfers from the Rh(III) center to the CO_2 first by the electrophilic attack of CO_2. Energy of 35.2 kcal/mol was cost for this intermolecular "direct" hydride transfer to form the cation metal formate complex **A11**, and this reaction barrier is higher than the rate determining step in Figure 1. Note that the "normal" CO_2 insertion mechanism is impossible because the dihydride complex **A2** is six coordinated and there is no vacant position for CO_2 to coordinate on metal center. Once the metal formate complex **A11** forms, two conceivable routes for the external base assisted second hydride abstraction are studied. One is the dissociation process in which $HCOO^-$ released from the Rh center of **A11** before the second hydride abstraction by base. This process leads to a very unstable intermediate **A12** with 33.3 kcal/mol Gibbs free energy relative to the reactants. The other is the association process in which the second hydride was abstracted by the base in the presence

of HCOO ligand in **A13**. This process goes through a transition state $\mathbf{TS_{A13\text{-}14}}$ with relative Gibbs free energy of 32.4 kcal/mol, which is lower than the energy of **A12** and the barrier of the previous hydride abstraction process. After the second hydride abstraction, barrierless release of $HCOO^-$ and $[HBase]^+$ occurs in order to finish the catalytic cycle. The TDTS for the pathway in Figure 2 is $\mathbf{TS_{A10\text{-}11}}$ and the energetic span (δE) is 35.2 kcal/mol, which is about 6.0 kcal/mol larger than that in Figure 1. Therefore, the pathway in Figure 2 cannot compete with the pathway in Figure 1.

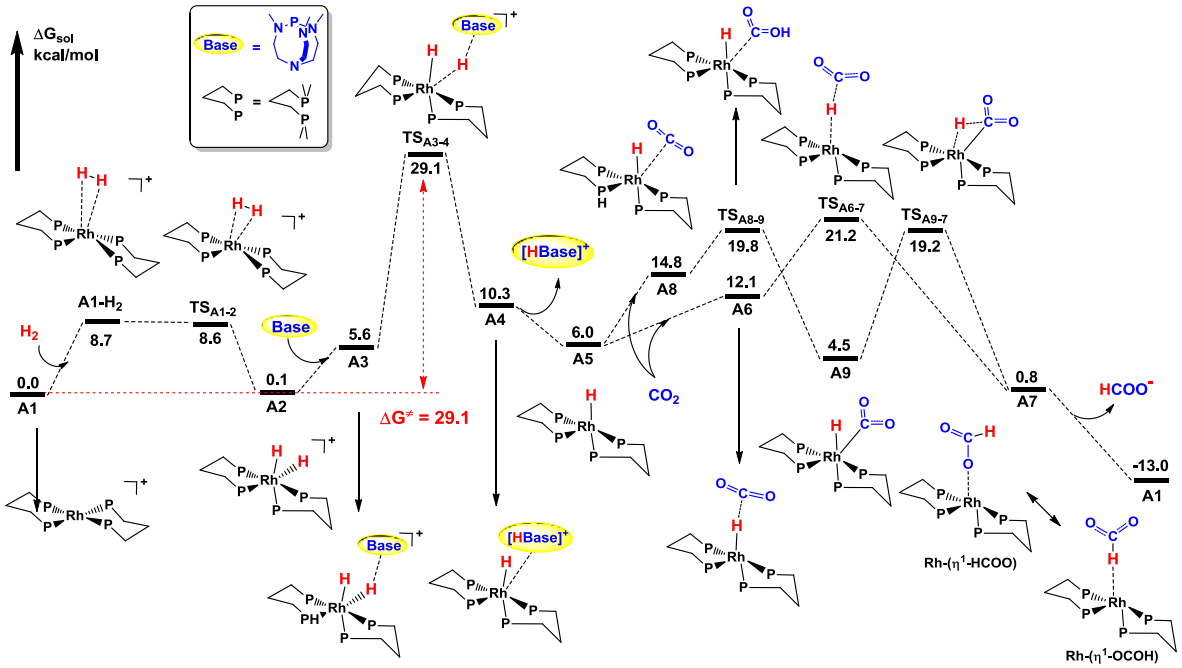

Figure 1. Solvent corrected Gibbs free energy profile for $[Rh(PCH_2CH_2CH_2P)_2]^+$ (**A1**) catalyzed CO_2 hydrogenation by the nucleophilic attack of Verkade's base to the hydride of the Rh dihydride complex.

Scheme 3 Molecular orbital interaction and electron transfer for electrophilic attack of CO_2 to metal hydride bond

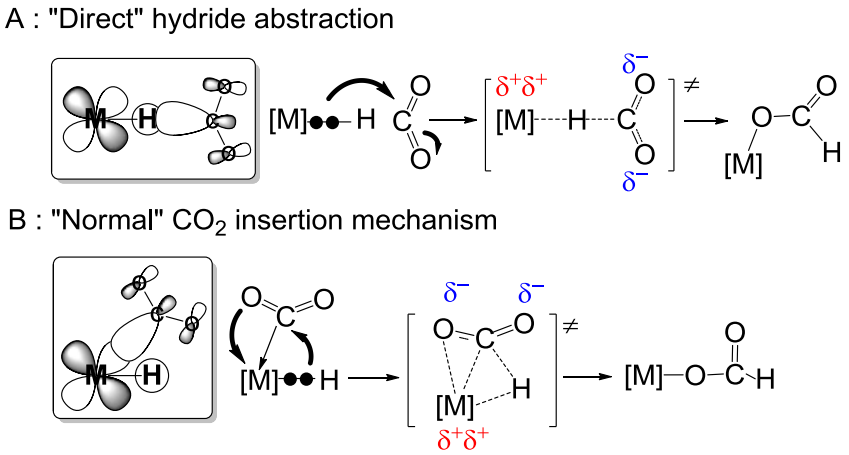

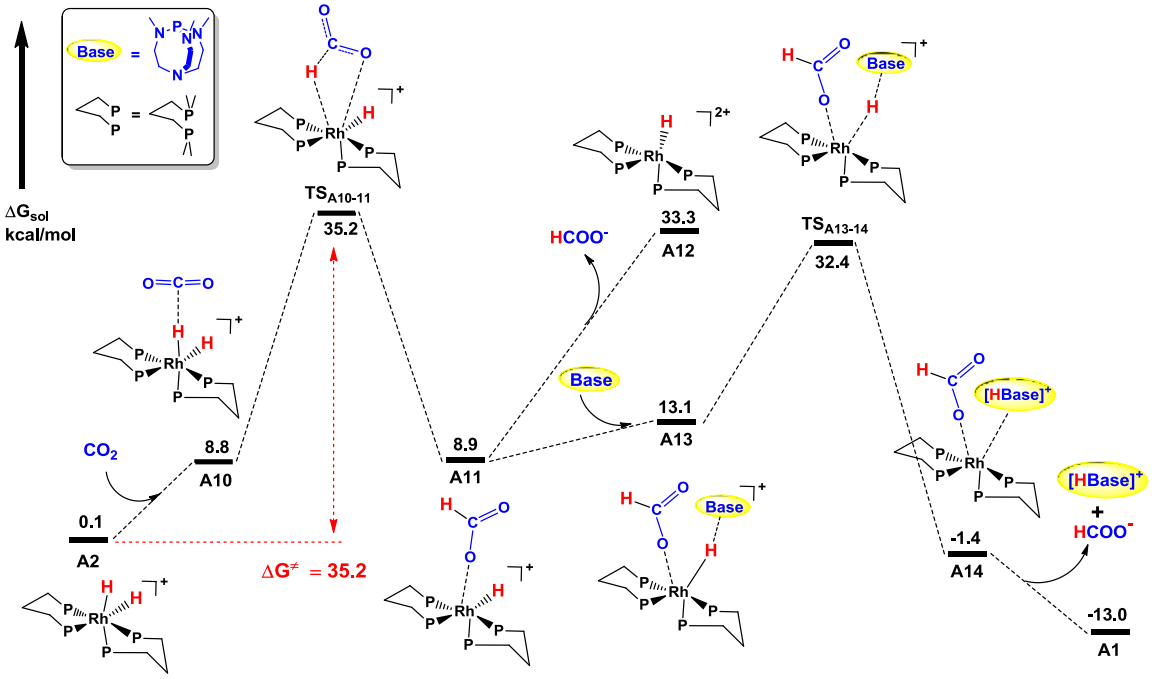

Figure 2. Solvent corrected Gibbs free energy profile for $[Rh(PCH_2CH_2CH_2P)_2]^+$ (**A1**) catalyzed CO_2 hydrogenation by the electrophilic attack of CO_2 to the hydride of the Rh dihydride complex.

3.2. $[Rh(PCH_2N^{Me}CH_2P)_2]^+$ (B1) catalyzed CO_2 hydrogenation

$[Rh(PCH_2N^{Me}CH_2P)_2]^+$ (B1) catalyzed CO_2 hydrogenation could have the similar inner sphere mechanism to that for **A1** catalyzed CO_2 hydrogenation. The energy profiles are displayed in Figures 3, S2, and S3. Quite similar to the mechanism in **A1** catalyzed CO_2 hydrogenation, sigma-complex **A1**-H_2 is also unstable and the overestimation of entropy effect in solvent makes it a little bit more unstable than $\mathbf{TS_{B1-2}}$ in solution phase free energy. **B1** catalyzed reaction occurs H_2 oxidative addition to Rh(I) center but through the $\mathbf{TS_{B1-2}}$ (9.4 kcal/mol) to form the 18e dihydride Rh(III) complex **B2**. Here, the higher H_2 oxidative addition reaction barrier than that in Figure 1 by 0.8 kcal/mol may be resulted from amine group which is introduced to the second coordination sphere. By overcoming the transition state $\mathbf{TS_{B3-4}}$ with a barrier of 26.0 kcal/mol, the first H-abstraction occurs by the nucleophilic attack of external Verkade's base and the unstable intermediate **B5** forms. After the first H-abstraction occurs, both "direct" hydride abstraction and "normal" CO_2 insertion into Rh-H to abstract the second hydride are studied. The barriers for the "direct" hydride abstraction and "normal" CO_2 insertion mechanism are 24.4 and 22.0 kcal/mol, respectively, indicating that the "normal" CO_2 insertion mechanism is more favorable due to an empty coordination site in metal center of **B8** for CO_2 to coordinate. However, these two barriers are all lower than that for the first H abstraction (26.0 kcal/mol in Figure 3). Facilely, after the second hydride abstraction by CO_2, rapid release of $HCOO^-$ and $[HBase]^+$ similar to that in Figure 1 occurs to regenerate the catalyst species, thus finishing the catalytic cycle. From the energetic span model[74,75,76,77], the TDTS in Figure 3 is $\mathbf{TS_{B3-4}}$ and the δE is about 26.0 kcal/mol. The δE is smaller than that in Figure 1 by about 3.1 kcal/mol, suggesting that the hydride in **B1** is easier to be abstracted than that in **A1**.

Here, we also studied the possible of σ-bond metathesis from **B7** with H_2 to regenerate **B5**. The calculated results in Figure S2 show that the barrier for this metathesis is higher than the one in the process to regenerate **B1** from **B5** in Figure 3, suggesting that **B5** catalyzed reaction cycle cannot compete with the one catalyzed by **B1.**

Figure S3 (Supporting Information) shows the alternative pathway for **B1** catalyzed CO_2 hydrogenation in which the first hydride of the dihydride complex **B2** is electrophilic attacked by CO_2 through a transition state $\mathbf{TS_{B10\text{-}11}}$ (38.7 kcal/mol) and the metal formate complex **B11** forms. The electrophilic attack of CO_2 on the pendant amine of diphosphine ligand seems possible if considering the frontier molecular orbital analysis of **B2** as shown in Figure S4. The HOMO and HOMO-1 of **B2** are mainly contributed by the diphosphine ligands with pendent amine, while the HOMO-2 of **B2** is the bonding interaction of s orbital of hydride and the d_z^2 orbital of Rh. Here, CO_2 cannot react with tertiary amine involving the molecular orbital interaction with HOMO or HOMO-1 of **B2** since there is no H in amine group. However the electrophilic attack of CO_2 to Rh-H bond involving HOMO-2 of **B2** is possible but with high reaction barrier as shown in Figure S3. Similar to the mechanism in Figure 2, the following dissociation of the formate leads to unstable rhodium hydride **B12.** Without the dissociation of the formate, the nucleophilic attack of Verkade's base to the Rh-H bond occurs in the presence of the coordination of the formate on the Rh center through a barrier of 28.4 kcal/mol, which is lower in energy than that of **B12** by 5.3 kcal/mol. After that, the formate and protonized base leave the metal center to regenerate the catalyst **B1**. Similarly, the TDTS for the reaction pathway in Figure S3 is the $\mathbf{TS_{B10\text{-}11}}$ corresponds to the first hydride abstraction by electrophilic attack of CO_2 (δE =

38.7 kcal/mol). Our theoretical investigation indicates that the pathway in Figure 3 is more favorable than the one in Figure S3.

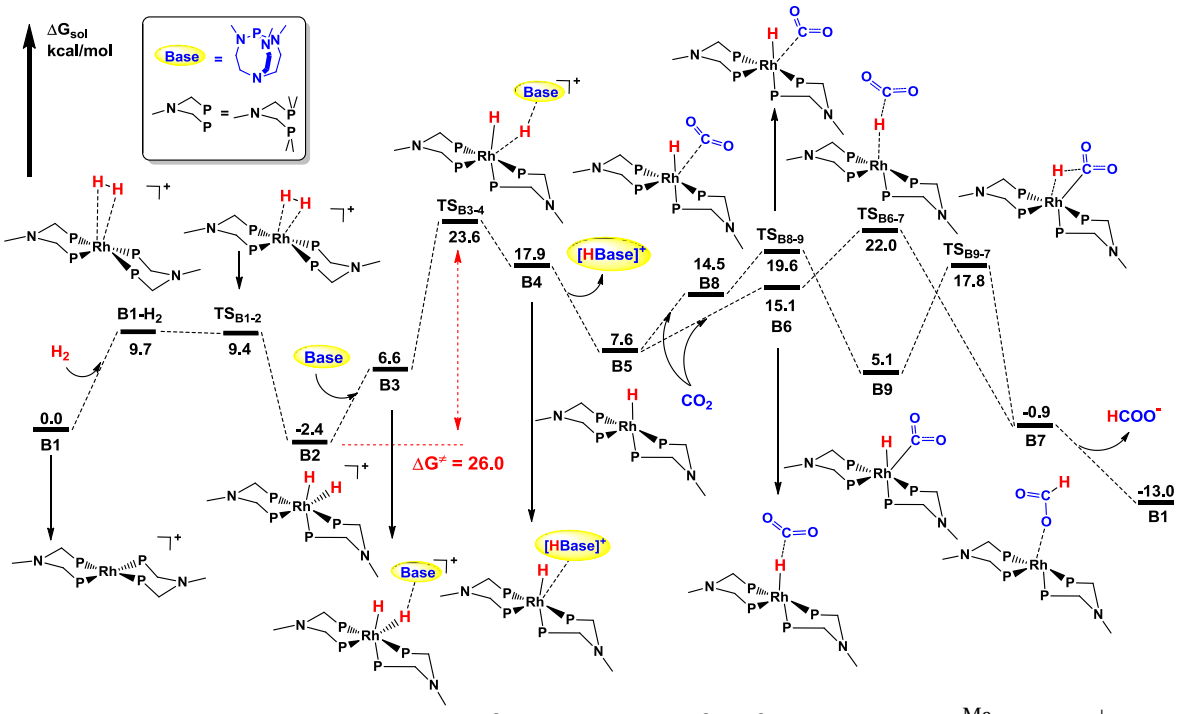

Figure 3. Solvent corrected Gibbs free energy profile for $[Rh(PCH_2N^{Me}CH_2P)_2]^+$ (**B1**) catalyzed CO_2 hydrogenation by the nucleophilic attack of Verkade's base to the hydride of the Rh dihydride complex.

For **B1** catalyzed CO_2 hydrogenation, one may ask about another conceivable route in which one hydrogen of the dihydride **B2** transfers to the outer sphere N atom of amine group as base. The composition of HOMO or HOMO-1 of **B2** shown in Figure S4 suggests that this H transfer is possible. Delightfully, this intramolecular H transfer occurs by overcoming a barrier of 20.8 kcal/mol ($\mathbf{TS_{B2\text{-}15}}$ in Figure S5) and an unstable **B15** forms with an unsaturated five coordinated Rh(III) center and oversaturated outer sphere amine group. **;**From this unstable intermediate **B15**, there are five possible routes leading to the

formation of the final product, which are summarized in Figure S6. In general, these pathways are proposed according the sequence of the attack of base and CO_2 on the metal hydride or amine proton. In case that the nucleophilic attack of base occurred firstly, two mechanisms with different intermolecular hydride abstraction are feasible. The first one is the hydride abstraction from Rh center to base via the transition state $\mathbf{TS_{B16\text{-}21}}$ as shown in Figure S5. By overcoming a barrier of 39.8 kcal/mol, unstable Rh(I) intermediate **B5** forms**.** From **B5**, rapid insertion of CO_2 to the Rh-H σ-bond and the succeeding barrierless formate elimination leads to the final products as in Figure 3. The TDTS of this route is TSB16-21 and the δE is calculated to be 39.8 kcal/mol, which is dramatically bigger than that of the mechanism in Figure 3 (26.0 kcal/mol). The second one is the hydride abstraction from the N atom to the base shown in Figure S6. This route goes through a very unstable intermediate **B17** (28.8 kcal/mol), which is also higher in energy than the total reaction barrier in Figure 3 (26.0 kcal/mol). Therefore, these two routes begin with the base's nucleophilic attack are both unfavorable and cannot compete with the pathway in Figure 3. As for the electrophilic attack of CO_2 on the metal hydride, there are also two possible routes as depicted in Figure S6. In these two routes, intermediates **B18** (30.5 kcal/mol) and **B19** (29.8 kcal/mol) are necessary to be passed over, which are all in very high energy. All of these calculated results show that the unstable **B15** preferred to be converted back to stable **B2** rather than being forwardly transformed to regenerate **B1** due to unstable intermediates or transition states for hydride abstraction by either base or CO_2. This result is consistent with the experimental observation[42] that no protonated amine was detected.

In 2011, a hydrogen bond donor in the second coordination sphere has been found to facilitate the CO_2 insertion by Hazari et al.[36,37] Prompted by this discovery, CO_2 insertion into metal hydride bond with the appearance of hydrogen bond donor from outer sphere amine was taken into consideration when we investigate the hydride abstraction from **B15** by CO_2. A transition state $\mathbf{TS_{B20\text{-}22}}$ is located as shown in Figure S5, indicating that the hydrogenation of CO_2 gives formic acid is finished in one step after one hydride transferred from metal to outer sphere amine. Unfortunately, the total reaction barrier is 42.2 kcal/mol, showing that this reaction pathway is not favorable, too.

From the discussion above, all the five outer sphere pathways derived from the intermediate **B15** cannot compete with the mechanism in Figure 3 although **B15** is formed via lower activation energy than the energetic span in Figure 3. Therefore, **B1** catalyzed CO_2 hydrogenation reaction prefers to happen by the three steps in Figure 3. The energetic span δE catalyzed by **B1** is 26.0 kcal/mol, which is 3.0 kcal/mol smaller than that catalyzed by **A1**. This agrees well with the experimental observation that the presence of N-CH_3 at the diphosphine ligand of **B1** enhanced the catalytic activity.[42] In order to figure out whether it is the π electron donating ability of amine group or σ electron withdrawing ability from electronegative N atom that influence the catalytic activity of Rh(diphosphine)$_2^+$, we used a model catalyst [Rh($PCH_2CF_2CH_2P)_2$]$^+$ (**C1**) with very strong σ electron withdrawing group CF_2 at the diphosphine ligand to compare.

3.3. [Rh($PCH_2CF_2CH_2P)_2$]$^+$ (C1) catalyzed CO_2 hydrogenation

$[Rh(PCH_2CF_2CH_2P)_2]^+$ (**C1**) catalyzed CO_2 hydrogenation is similar to the inner sphere mechanism in Figures 1 and 3, **C1** catalyzed reaction also begins with the pre-coordinate of H_2 to **C1**. The unstable sigma-complex **C1-H$_2$** is higher in solvent corrected Gibbs free energy than that of **TS$_{C1-2}$** because of the overestimation of entropy effect. The oxidative addition of H_2 to Rh(I) center to form a 18e Rh(III) dihydride intermediate **C2**. As shown in Figure 4, the barrier for this H_2 addition step is 10.0 kcal/mol. This barrier is a little bit higher than H_2 addition barriers in Figures 1 and 3, which may be caused by the strong electron withdrawing CF_2 group makes the metal center more electron deficient than those in **A1** and **B1**. Thus, the back donating from metal center to H_2 is less sufficient in **TS$_{C1-2}$** than that in **TS$_{A1-2}$** and **TS$_{B1-2}$**. The release of the first hydride by the nucleophilic attack of base needs to overcome the transition state **TS$_{C3-4}$** with a barrier of 18.0 kcal/mol. Once the monohydride metal complex **C5** forms, the second hydride could be abstracted rapidly by the electrophilic attack of CO_2 and the metal formate intermediate forms. Here, either "direct" hydride abstraction by CO_2 or "normal" CO_2 insertion into Rh-H bond overcomes lower reaction barrier than the previous first hydride abstraction step. Obviously, the transition state **TS$_{C3-4}$** corresponds to the first hydride abstraction by nucleophilic attack of base is also the TDTS in this route with a calculated energetic span δE of 18.0 kcal/mol. And this energetic span is much smaller than those in Figures 1 and 3, showing enhanced catalytic activity of **C1**.

Here, we also studied the possible of σ-bond metathesis from **C7** with H_2 to regenerate **C5** as an active species. The calculated results in Figure S7 show that the barrier for this

metathesis is higher than the one in the process to regenerate **C1** from **C5** in Figure 4 , suggesting that **C5** catalyzed reaction cycle cannot compete with the one catalyzed by **C1.**

In Figure S8, the first hydride abstraction by the electrophilic attack of CO_2 through $\mathbf{TS_{C10\text{-}11}}$ needs a very high barrier of 39.3 kcal/mol. The succeeding second hydride abstraction via association mode by nucleophilic attack of Verkade's base is easier than the first hydride abstraction by CO_2. However, the energetic span of this route is obviously smaller than that in Figure 4, which makes the **C1** catalyzed reaction prefer to go through the pathway in Figure 4.

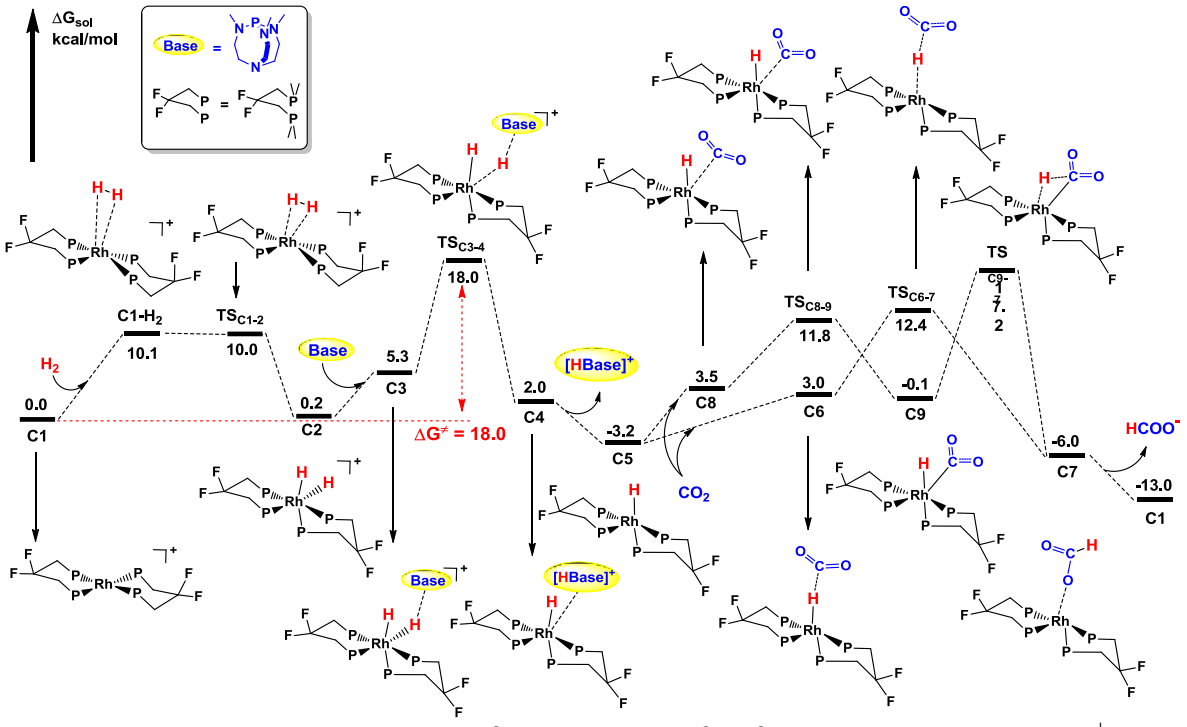

Figure 4. Solvent corrected Gibbs free energy profile for $[Rh(PCH_2CF_2CH_2P)_2]^+$ (**C1**) catalyzed CO_2 hydrogenation by the nucleophilic attack of Verkade's base to the hydride of the Rh dihydride complex.

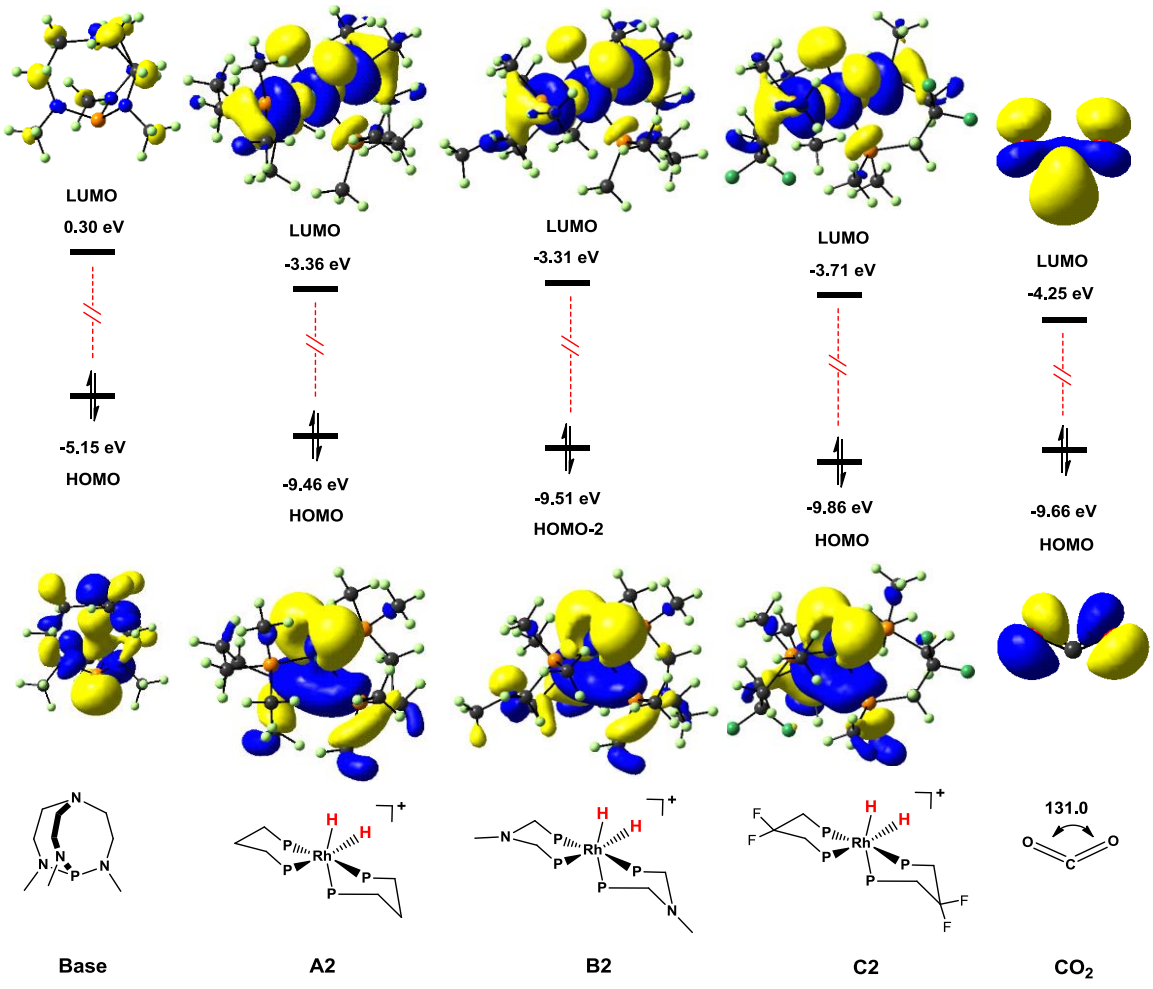

Figure 5. Skeleton diagrams and energies (in eV) of frontier molecular orbitals for Verkade's base, **A2**, **B2**, **C2**, and bent CO_2.

A1, **B1**, and **C1** catalyzed CO_2 hydrogenation reactions undergo similar favorable pathways in which H_2 oxidative addition occurs first, and the first metal hydride is abstracted by the Verkade's base followed by electronic attack of CO_2 on the second metal hydride from unstable five coordinated Rh complexes. The reactions are assumed beginning with H_2 oxidative addition because these reaction barriers are very small when compare with other processes such as H_2 addition to Rh-H and Rh-OCHO complexes

(Figures S1, S2, S7). At the same time, NBO charge distribution in **A2**, **B2**, and **C2** showns that the H atoms on the metal center are both weak hydridic by carrying less than -0.1 charge (Figure S9), that's why the weaker hydridic one can be attacked by very strong base. When we analyze the structural parameters of these structures, we found that the M-H bonds are about 1.580Å and the H-H bonds are about 2.100 Å, showing that H_2-Rh complex is not Kubas type, but metal dihydride.

The TDTSs are all corresponds to the first hydride abstraction by the nucleophilic attack of the base. The energetic span δE decrease from 29.1, 26.0 to 18.0 kcal/mol when the reactions are catalyzed by **A1**, **B1**, and **C1**. This can be well understood by the frontier molecular orbitals analysis shown in Figure 5.[78] It is shown in Figure 5 that the *p* orbital of P atom in the HOMO (highest occupied molecular orbital) of Verkade's base has the same symmetry as the LUMO (lowest unoccupied molecular orbital) of Rh dihydride complexes, which is the antibonding interaction between the *s* orbital of hydride and the d_z^2 orbital of Rh, thus allowing nucleophilic attack. The energy differences between the HOMO of Verkade's base and LUMOs of Rh dihydride complexes are smaller than those between the LUMO of Verkade's base and HOMO of Rh dihydride complexes. Therefore the reaction of Verkade's base and the Rh dihydride complexes occur by the interaction between the HOMO of base and LUMOs of **A2, B2**, and **C2** as a nucleophilic attack. The energy difference between the HOMO of base and LUMOs of **C2** is smaller than that of **A2** and **B2** which makes the nucleophilic attack of Verkade's base to hydride of **C2** more favorable than those of **A2** and **B2**. By contrast, CO_2 is usually considered as electron deficient compound. The bent CO_2 is more active than the linear CO_2 because the lowered LUMO

makes it convenient to experience electrophilic attack. The frontier molecular orbitals of CO_2 are obtained from the geometry of bend CO_2 in $\mathbf{TS_{C10\text{-}11}}$. The *p* orbital of C atom in bent CO_2 contributes most in its LUMO, showing this is the most electron deficient site. HOMO-2 of **B2** is the bonding interaction of *s* orbital of hydrogen atom and the d_z^2 orbital of Rh center. The interaction of LUMO of bent CO_2 with the HOMO (**A2** and **C2**) or HOMO-2 (**B2**) is symmetry allowed. At the same time the energy differences between the LUMO of bent CO_2 and HOMOs/HOMO-2 of Rh dihydride complexes are smaller than those between the HOMO of bent CO_2 and LUMOs of Rh dihydride complexes accordingly. Therefore, electrophilic attack of CO_2 to the Rh dihydride complexes is also possible. However, the energy differences between the LUMO of bent CO_2 and HOMOs/HOMO-2 of Rh dihydride complexes (5.21, 5.26, and 5.61 eV for **A2**, **B2**, and **C2**) are significantly larger than the energy differences between the HOMO of Verkade's base and LUMOs of Rh dihydride complexes (1.79, 1.84, and 1.44 eV for **A2**, **B2**, and **C2**). This comparison confirms that the nucleophilic attack of Verkade's base to Rh dihydride complexes is more favorable than the electrophilic attack of CO_2 to Rh dihydride complexes. The frontier molecular orbital analysis results confirms the calculated energy profiles shown in previous figures that the first hydride abstractions by the base have lower barriers (29.1, 26.0, and 18.0 kcal/mol for **A2**, **B2**, and **C2**) than the electrophilic attack of CO_2 (35.2, 38.7, and 39.3 kcal/mol barriers for **A2**, **B2**, and **C2**).

3.4. Origin of substituent Effects on the catalytic activity

Origin of substituent Effects on the catalytic activity of Rh diphosphine complexes for CO_2 hydrogenation could be well addressed by the investigation of the relationships

between the electronic structure of the substituents in the bidentate phosphine ligand and the thermodynamic hydricity of the transition metal hydride. Hydricity including thermodynamic hydricity and kinetic hydricity has been deeply investigated both experimentally and theoretically[79,80,81] and this parameter is used in the investigation of CO_2 hydrogenation.[82,83] The thermodynamic hydricity describes the hydride donor ability of the M-H bond. It is obvious that the larger the hydricity of the metal hydride complex, the stronger the hydride donor ability of metal hydride bond and easier the hydride to be abstracted by nucleophiles such as base. The thermodynamic hydricity is the standard Gibbs free energy change ($\Delta G_H^{-\circ}$) of Rea.1. $\left[Pt(dmpp)_2\right]^{2+}$ is used as a reference complex to make the charge distribution balanced in both sides of the equation, thus Rea.2 was given,

$$\left[(PX^RP)_2RhH_2\right]^+ \rightarrow \left[(PX^RP)_2RhH\right]^{2+} + H^- \qquad \textbf{Rea.1}$$

$$\left[(PX^RP)_2RhH_2\right]^+ + \left[Pt(dmpp)_2\right]^{2+} \rightarrow \left[(PX^RP)_2RhH\right]^{2+} + \left[HPt(dmpp)_2\right]^+ \qquad \textbf{Rea.2}$$

where the Gibbs free energy change of this isodesmic reaction is $\Delta G_{exchange}$. Therefore, the $\Delta G^{\circ}_{H^-}(\left[(PX^RP)_2RhH_2\right]^+)$ could be obtained by the Equation 3:

$$\Delta G^{\circ}_{H^-}(\left[(PX^RP)_2RhH_2\right]^+) = \Delta G^{\circ}_{H^-}(\left[HPt(dmpp)_2\right]^+) + \Delta G_{exchange} \qquad \textbf{Eq. 3}$$

where $\Delta G^{\circ}_{H^-}(\left[HPt(dmpp)_2\right]^+)$ = 50.7 kcal/mol in acetonitrile according to the experiment.[71,84]

Here, we use the thermodynamic hydricity of the transition metal hydride **A2**, **B2**, and **C2** to explain the reasons leading to the differences of catalytic activity. The $\Delta G^{\circ}_{H^-}(\left[(PX^RP)_2RhH_2\right]^+)$ of **A2**, **B2**, and **C2** are calculated[71] to be 73.5, 77.5, and 80.5 kcal/mol, respectively in Table 1. The hydricity order of these three complexes is consistent with the order of energetic span δE for three favorable pathway respectively and in agreement with the σ electron withdrawing order of three substitutes that CH_2 < N-CH_3 < CF_2. We should bear in mind that the attack by the Verkade's base is a nucleophile while CO_2 is an electrophile to insert into metal hydride bond. The increased thermodynamic hydricity from **A2**, **B2** to **C2** make the nucleophilic attack of Verkade's base to hydride more and more favorable; instead, the electrophilic attack of CO_2 to metal hydride bond becomes more and more difficult. These analysis well explain the calculated results that the barrier of the first hydride abstraction by base decreases from catalyst **A1** (29.1 kcal/mol), **B1** (26.0 kcal/mol) to **C1** (18.0 kcal/mol), while the first hydride transfer barriers by the nucleophilic attack of CO_2 increase from catalyst **A1** (35.2 kcal/mol), **B1** (38.7 kcal/mol) to **C1** (39.3 kcal/mol). Therefore, it is the σ electron withdrawing ability rather than the π electron donating ability that lowered the activation barrier of Rh(diphosphine)$_2^+$ catalysed CO_2 hydrogenation.

Table1. Calculated thermodynamic hydricity $\Delta G^{\circ}_{H^-}(\left[(PX^RP)_2RhH_2\right]^+)$ for dihydride complexes **A2**, **B2**, and **C2**.

Transiton-metal dihydride	$\Delta G^{\circ}_{H^-}([(PX^RP)_2RhH_2]^+)$ (kcal/mol)
A2 : $[H_2Rh(PCH_2CH_2CH_2P)_2]^+$	73.5
B2 : $[H_2Rh(PCH_2N^{Me}CH_2P)_2]^+$	77.5
C2 : $[H_2Rh(PCH_2CF_2CH_2P)_2]^+$	80.5

4. Conclusion

In this work, detailed mechanism of 16e catalysts $[Rh(PCH_2CH_2CH_2P)_2]^+$ (**A1)**, $[Rh(PCH_2N^{Me}CH_2P)_2]^+$ (**B1)**, and $[Rh(PCH_2CF_2CH_2P)_2]^+$ (**C1**) catalyzed CO_2 hydrogenation and the influences of the substituents at the diphosphine ligand to the catalytic activities are examined by DFT calculations. Our calculations show that catalytic reactions start with the H_2 oxidative addition to the Rh(I) center of the catalyst to give the 18e Rh(III) dihydride complex, and go ahead with the first hydride abstraction by nucleophilic attack of the external Verkade's base, finishing by the second hydride abstraction by electrophilic attack of CO_2 and subsequent release of formate and protonated base. The TDTS in the most favorable pathway is the first hydride abstraction by the Verkade's base, while the reactions for H_2 oxidative addition and the release of the second hydride proceed faster with lower activation energies. The calculated results show that the energetic span δE decrease from **A1**, **B1** to **C1**, which agrees well with the experimental result that **B1** has better catalytic activities than **A1**. In contract to the previous experimental view that the electron donating group N-CH_3 at the bidentate phosphine ligand increased the efficiency of the catalyst, we find it is σ electron withdrawing ability that enhanced the catalytic efficiency. This opinion is confirmed by

using **C1** as the model catalyst in our theoretical study. The comparison of the different reaction barriers is consistent with the molecular orbital analysis and the order of energetic span is well explained by the thermodynamic hydricity order of Rh dihydride complexes with different substitutes at diphosphine ligand. Our study suggests a new catalyst for CO_2 hydrogenation and refreshes the understanding of the electronic effect of substituent at the bidentate phosphine ligand.

Acknowledgement. Financial support from Shenzhen special funds for the development of new energy (No. JCYJ20140714151402764) and the National Natural Science Foundation of China (No. 21573102), L. D. is thankful to Southern University of Science and Technology.

Supporting Information Available: Complete Ref. 44, figures of optimized compounds/intermediates and transition states, tables of relative electronic and free energies in gas phase and relative electronic energy in solution phase, along with cartesian coordinates and electronic energies for all of the calculated structures. This material is available free of charge via the Internet at http://pubs.rsc.org.

References

[1] R. H. Ma, G. F. Schuette, L. J. Broadbelt, J. Catal. 317 (2014) 176.

[2] A. M. Appel, J. E. Bercaw, A. B. Bocarsly, H. Dobbek, D. L. DuBois, M. Dupuis, J. G. Ferry, E. Fujita, R. Hille, P. J. A. Kenis, C. A. Kerfeld, R. H. Morris, C. H. F. Peden, A. R. Portis, S. W. Ragsdale, T. B. Rauchfuss, J. N. H. Reek, L. C. Seefeldt, R. K. Thauer, G. L. Waldrop, Chem. Rev. 113 (2013) 6621.

[3] X. Jiang, F. L. Gou, H. W. Jing, J. Catal. 313 (2014) 159.

[4] E. Balaraman, C. Gunanathan, J. Zhang, L. J. W. Shimon, D. Milstein, Nat. Chem. 3 (2011) 609.

[5] S. Chakraborty, J. Zhang, J. A. Krause, H. R. Guan, J. Am. Chem. Soc. 132 (2010) 8872.

[6] B. Mutz, H. W. P. Carvalho, S. Mangold, W. Kleist., J. D. Grunwaldt, J. Catal. 327 (2015) 48.

[7] A. Berkefeld, W. E. Piers, M. Parvez, L. Castro, L. Maron, O. Eisenstein, Chem. Sci. 4 (2013) 2152.

[8] S. M. Glueck, S. Gumus, W. M. F. Fabian, K. Faber, Chem. Soc. Rev. 39 (2010) 313.

[9] K. Schuchmann, V. Müller, Science 342 (2013) 1382.

[10] G. Bredig, S. R. Carter, Berichte 47 (1914) 541.

[11] M. W. Farlow, H. Adkins, J. Am. Chem. Soc. 57 (1935) 2222.

[12] Y. Inoue, H. Izumida, Y. Sasaki, H. Hashimoto, Chem. Lett. 5 (1976) 863.

[13] J. Elek, L. Nadasdi, G. Papp, G. Laurenczy, F. Joó, Appl. Catal. A-Gen. 255 (2003) 59.

[14] A. Boddien, F. Gärtner, C. Federsel, P. Sponholz, D. Mellmann, R. Jackstell, H. Junge, M. Beller, Angew. Chem., Int. Ed. 50 (2011) 6411.

[15] S. Sanz, A. Azua, E. Peris, Dalton Trans. 39 (2010) 6339.

[16] G. A. Filonenko, D. Smykowski, B. M. Szyja, G. Li, J. Szczygieł, E. J. M. Hensen, . E. A. Pidko, ACS Catal. 5 (2015) 1145.

[17] N. N. Ezhova, N. V. Kolesnichenko, A. V. Bulygin, E. V. Slivinskii, S. Han, Russ. Chem. Bull. 51 (2002) 2165.

[18] F. Gassner, W. Leitner, Chem. Commun. 19 (1993) 1465.

[19] F. Hutschka, A. Dedieu, M. Eichberger, R. Fornika, W. Leitner, J. Am. Chem. Soc. 119(1997) 4432.

[20] F. Hutschka, A. Dedieu, W. Leitner, Angew. Chem. Int. Ed. 34 (1995) 1742.

[21] Y. Musashi, S. Sakaki, J. Am. Chem. Soc. 124 (2002) 7588.

[22] I. Jószai, F. Joó, J. Mol. Catal. A: Chem. 224 (2004) 87.

[23] R. Tanaka, M. Yamashita, K. Nozaki, J. Am. Chem. Soc. 131 (2009) 14168.

[24] C. Liu, J. H. Xie, G. L. Tian, W. Li, Q. L. Zhou, Chem. Sci. 6 (2015) 2928.

[25] R. Langer, Y. Diskin-Posner, G. Leitus, L. J. W. Shimon, Y. Ben-David, D. Milstein, Angew. Chem., Int. Ed. 50 (2011) 9948.

[26] M. S. G. Ahlquist, J. Mol. Catal. A: Chem. 324 (2010) 3.

[27] X. Z. Yang, ACS Catal. 1 (2011) 849.

[28] G. Manca, I. Mellone, F. Bertini, M. Peruzzini, L. Rosi, D. Mellmann, H. Junge, M. Beller, A. Ienco, L. Gonsalvi, Organometallics 32 (2013) 7053.

[29] C. Hou, J. X. Jiang, S. D. Zhang, G. Wang, Z. H. Zhang, Z. F. Ke, C. Y. Zhao, ACS Catal. 4 (2014) 2990.

[30] G. A. Filonenko, E. J. M. Hensen, E. A. Pidko, Catal. Sci. Technol. 4 (2014) 3474.

[31] A. Urakawa, F. Jutz, G. Laurenczy, A. Baiker, Chem. Eur. J. 13 (2007) 3886.

[32] N. Kumar, D. M. Camaioni, M. Dupuis, S. Raugei, A. M. Appel, Dalton Trans. 43 (2014) 11803.

[33] W. H. Bernskoetter, N. Hazari, Eur. J. Inorg. Chem. (2013) 4032.

[34] R. Tanaka, M. Yamashita, L. W. Chung, K. Morokuma, K. Nozaki, Organometallics 30 (2011) 6742.

[35] T. Fan, X. H. Chen, Z. Y. Lin, Chem. Commun. 48 (2012) 10808.

[36] T. J. Schmeier, G. E. Dobereiner, R. H. Crabtree, N. Hazari, J. Am. Chem. Soc. 133 (2011) 9274.

[37] A. M. Lilio, M. H. Reineke, C. E. Moore, A. L. Rheingold, M. K. Takase, C. P. Kubiak, J. Am. Chem. Soc. 137 (2015) 8251.

[38] W. H. Wang, J. F. Hull, J. T. Muckerman, E. Fujita, Y. Himeda, Energy Environ. Sci. 5 (2012) 7923.

[39] E. Fujita, J. T. Muckerman, Y. Himeda, Biochimica et Biophysica Acta 1827 (2013) 1031.

[40] W. H. Wang, J. T. Muckerman, E. Fujita, Y. Himeda, ACS Catal. 3 (2013) 856.

[41] N. Onishi, S. A. Xu, Y. Manaka, Y. Suna, W. H. Wang, J. T. Muckerman, E. Fujita, Y. Himeda, Inorg. Chem. 54 (2015) 5114.

[42] J. T. Bays, N. Priyadarshani, M. S. Jeletic, E. B. Hulley, D. L. Miller, J. C. Linehan, W. J. Shaw, ACS Catal. 4 (2014) 3663.

[43] J. D. Chai, M. Head-Gordon, Phys. Chem. Chem. Phys. 10 (2008) 6615.

[44] M. J. Frisch, Gaussian, Inc., Wallingford CT, (2009).

[45] P. J. Hay, W. R. Wadt, J. Chem. Phys. 82 (1985) 270.

[46] W. R. Wadt, P. J. Hay, J. Chem. Phys. 82 (1985) 284.

[47] P. J. Hay, W. R. Wadt, J. Chem. Phys. 82 (1985) 299.

[48] C. E. Check, T. O. Faust, J. M. Bailey, B. J. Wright, T. M. Gilbert, L. S. Sunderlin, J. Phys. Chem. A 105 (2001) 8111.

[49] A. W. Ehlers, M. BÖhme, S. Dapprich, A. Gobbi, A. HÖllwarth, V. Jonas, K. F. KÖhler, R. Stegmann, A. Veldkamp, G. Frenking, Chem. Phys. Lett. 208 (1993) 111.

[50] A. HÖllwarth, M. BÖhme, S. Dapprich, A. W. Ehlers, A. G. Obbi, V. Jonas, K. F. KÖhler, R. Stegmann, A. Veldkamp, G. Frenking, Chem. Phys. Lett. 208 (1993) 237.

[51] P. C. Hariharan, J. A. Pople, Theor. Chim. Acta 28 (1973) 213.

[52] M. S. Gordon, Chem. Phys. Lett. 76 (1980) 163.

[53] R. C. J. Binning, L. A. Curtiss, J. Comput. Chem. 11 (1990) 1206.

[54] W. Y. Hung, B. Liu, W. Shou, T. B. Wen, C. Shi, H. H. Y. Sung, I. D. Williams, Z. Y. Lin, G. C. Jia, J. Am. Chem. Soc. 133 (2011) 18350.

[55] X. F. Tan, Y. Wang, Y. H. Liu, F. Y. Wang, L. Y. Shi, K. H. Lee, Z. Y. Lin, H. Lv, X. M. Zhang, Org. Lett. 17 (2015) 454.

[56] T. D. Wang, H. Zhang, F. F. Han, L. P. Long, Z. Y. Lin, H. P. Xia, Chem. Eur. J. 19 (2013) 10982.

[57] T. Ghebreghiorgis, B. Biannic, B. H. Kirk, D. H. Ess, A. Aponick, J. Am. Chem. Soc. 134 (2012) 16307.

[58] A. Friedrich, M. Drees, J. S. A. D. Günne, S. Schneider, J. Am. Chem. Soc. 131 (2009) 17552.

[59] K. Fukui, J. Phys. Chem. 74 (1970) 4161.

[60] K. Fukui, Acc. Chem. Res. 14 (1981) 363.

[61] A. V. Marenich, C. J. Cramer, D. G. Truhlar, J. Phys. Chem. B 113 (2009) 6378.

[62] G. Y. Yin, I. Kalvet, U. Englertn, F. Schoenebeck, J. Am. Chem. Soc. 137 (2015) 4164.

[63] S. R. Neufeldt, G. Jiménez-Osés, J. R. Huckins, O. R. Thiel, K. N. Houk, J. Am. Chem. Soc. 137 (2015) 9843.

[64] G. Jindal, R. B. Sunoj, J. Am. Chem. Soc. 136 (2014) 15998.

[65] Q. Q. Lu, H. Z. Yu, Y. Fu, J. Am. Chem. Soc. 136 (2014) 8252.

[66] A. Fromm, C. V. Wüllen, D. Hackenberger, L. J. Gooßen, J. Am. Chem. Soc. 136 (2014) 10007.

[67] Y. Y. Jiang, Q, Zhang, H. Z. Yu, Y. Fu, ACS Catal. 5 (2015) 1414.

[68] G. J. Cheng, Y. F. Yang, P. Liu, P. Chen, T. Y. Sun, G. Li, X. H. Zhang, K. N. Houk, J. Q. Yu, Y. D. Wu, J. Am. Chem. Soc. 136 (2014) 894.

[69] P. Liu, L. E. Sirois, P. H. Y. Cheong, Z. X. Yu, I. V. Hartung, H. Rieck, P. A. Wender, K. N. Houk, J. Am. Chem. Soc. 132 (2010) 10127.

[70] X. F. Xu, P. Liu, A. Lesser, L. E. Sirois, P. A. Wender, K. N. Houk, J. Am. Chem. Soc. 134 (2012) 11012.

[71] X. J. Qi, Y. Fu, L. Liu, Q. X. Guo, Organometallics 26 (2007) 4197.

[72] CYLview, 1.0b; C. Y. Legault, Université de Sherbrooke, (2009) (http://www.cylview.org)

[73] Parameters comes from database of the National Institute of Standards and Technology

(http://webbook.nist.gov/)

[74] S. Kozuch, S. Shaik, J. Am. Chem. Soc. 128 (2006) 3355.

[75] A. Uhe, S. Kozuch, S. Shaik, J. Comput. Chem. 32 (2011) 978.

[76] S. Kozuch, S. Shaik, Acc. Chem. Res. 44 (2011) 101.

[77] S. Kozuch, J. M. L. Martin, ACS Catal. 2 (2012) 2787.

[78] The skeleton diagrams and energies of frontier molecular orbitals are calculated by B3LYP functional (Single point calculation based on the gas phase optimized geometries at ωb97xd).

[79] T. Y. Cheng, B. S. Brunschwig, R. M. Bullock, J. Am. Chem. Soc. 120 (1998) 13121.

[80] R. M. Bullock, A. M. Appel, M. L. Helm, Chem. Commun. 50 (2014) 3125.

[81] Y. Matsubara, E. Fujita, M. D. Doherty, J. T. Muckerman, C. Creutz, J. Am. Chem. Soc. 134 (2012) 15743.

[82] D. L. DuBois, D. E. Berning Appl. Organometal. Chem. 14 (2000) 860.

[83] J. T. Muckermanl, P. Achord, C. Creutz, D. E. Polyansky, E. Fujita Proc. Natl. Acad. Sci. USA 109 (2012) 15661.

[84] C. J. Curtis, A. Miedaner, W. W. Ellis, D. L. DuBois, J. Am. Chem. Soc. 124 (2002) 1918.